J|A|C|S
ARTICLES
Published on Web 08/10/2002

Charge-Transfer Transitions in Triarylamine Mixed-Valence Systems: A Joint Density Functional Theory and Vibronic Coupling Study

V. Coropceanu, M. Malagoli, J. M. André,† and J. L. Brédas*

Contribution from the Department of Chemistry, The University of Arizona, Tucson, Arizona 85721-0041

Received April 5, 2002

Abstract: A theoretical model is developed to describe the intramolecular transfer in organic mixed-valence systems. It is applied to rationalize the intervalence charge-transfer transitions in triarylamine mixed-valence compounds. The electronic coupling parameter is evaluated at the density functional theory (DFT) and time-dependent density functional theory (TD-DFT) levels. The shapes of the charge-transfer absorption bands are analyzed in the framework of a dynamic vibronic model. The influence on the optical properties of diagonal and nondiagonal vibronic couplings is discussed. Our results are compared to recent experimental data.

I. Introduction

The understanding and control of electron-transfer (ET) processes in biological, physical, and chemical systems continue to be among the most active research areas.[1] In the study of intramolecular ET, mixed-valence (MV) systems are especially valuable; these are systems that contain two or more redox states within the same molecule or molecular unit.[2−8] Among the MV compounds, the dimeric systems are the most extensively studied, such as the well-known Creutz−Taube ion,[9] $[(NH_3)_5$-Ru-pyrazine-Ru$(NH_3)_5]^{5+}$. These constitute the most simple electron-transfer systems as they consist of only two charge-bearing subunits M_a^n and M_b^{n+1}, one with oxidation state n and the other with oxidation state $n + 1$; these subunits can be linked directly or via a bridging ligand L_i. The properties of MV systems depend strongly on the extent of electronic interaction between subunits M_a^n and M_b^{n+1}. The magnitude of this interaction is defined by the matrix element $H_{ab} = \langle\Psi_a|H|\Psi_b\rangle$, where H is the molecular Hamiltonian, and Ψ_a and Ψ_b are two localized states (termed diabatic states) corresponding, in the hypothetical absence of any coupling between the subunits, to two localized valence structures $M_a^{n+1}-L_i-M_b^n$ and $M_a^n-L_i-M_b^{n+1}$. In accordance with the common classification, MV systems are divided into three classes: class I, complete valence trapping (negligible electronic coupling between the two redox sites); class II, valence trapping (weak electronic coupling); and class III, delocalized valency (strong electronic coupling).[10]

A very important feature of the class II and class III MV complexes is the appearance in the visible or the near-infrared region of an absorption band called the intervalence transfer or charge-transfer (CT) band, which cannot be attributed to the system subunits or to the bridging ligands. Of greatest interest is the fact that from the CT band it is possible to estimate the two basic parameters, that is, the electronic coupling H_{ab} and the reorganization energy λ, that in the semiclassical Marcus model determine the rate constant of the self-exchange electron-transfer process.[11]

For the weak coupling case (class II systems), Hush has shown[12] that the maximum of the CT band, E_{op}, is equal to the Marcus reorganization energy[11] λ:

$$E_{op} = h\nu_{max} = \lambda \quad (1)$$

* To whom correspondence should be addressed. E-mail: jlbredas@u.arizona.edu.
† Permanent address: Laboratoire de Chimie Théorique Appliquée, Facultés Universitaires Notre-Dame de la Paix, B-5000 Namur, Belgium.

(1) Electron Transfer: From Isolated Molecules to Biomolecules. *Adv. Chem. Phys.*; Bixon, M., Jortner, J., Eds.; Wiley: New York, 1999; Vols. 106, 107.
(2) *Mixed-Valence Compounds: Theory and Applications in Chemistry, Physics, Geology, and Biology*; Brown, D. B., Ed.; D. Reidel Academic Publishers: Dordrecht, 1980.
(3) *Mixed Valency Systems. Applications in Chemistry, Physics, and Biology*; Prassides, K., Ed.; Kluwer Academic Publishers: Dordrecht, 1991.
(4) (a) Creutz, C. *Prog. Inorg. Chem.* **1983**, *30*, 1. (b) Richardson, D. E.; Taube, H. *Coord. Chem. Rev.* **1984**, *60*, 107. (c) Brunschwig, B. S.; Creutz, C.; Sutin, N. *Chem. Soc. Rev.* **2002**, *31*, 168.
(5) (a) Trautwein, A. X.; Bill, E.; Bominaar, E. L.; Winkler, H. *Struct. Bonding* **1991**, *78*, 1. (b) Astruc, D. *Electron Transfer and Radical Processes in Transition-Metal Chemistry*; VCH Publishers: New York, 1995. (c) Crutchley, R. J. *Adv. Inorg. Chem.* **1994**, *41*, 273−325. (d) Bersuker, I. B.; Borshch, S. A. *Adv. Chem. Phys.* **1992**, *81*, 703.
(6) (a) Newton, M. D. *Chem. Rev.* **1991**, *91*, 767. (b) Creutz, C.; Newton, M. D.; Sutin, N. *J. Photochem. Photobiol., A* **1994**, *82*, 47. (c) Cave, R. J.; Newton, M. D. *Chem. Phys. Lett.* **1996**, *249*, 15.
(7) (a) Barbara, P. F.; Meyer, T. J.; Ratner, M. A. *J. Phys. Chem.* **1996**, *100*, 13148. (b) Demadis, K. D.; Hartshorn, C. M.; Meyer, T. J. *Chem. Rev.* **2001**, *101*, 2655.
(8) (a) Coropceanu, V.; Brédas, J. L.; Winkler, H.; Trautwein, A. X. *J. Chem. Phys.* **2002**, *116*, 8152. (b) Coropceanu, V. P.; Prassides, K. *Chem. Phys. Lett.* **1988**, *289*, 53. (c) Coropceanu, V. P.; Bordian, V. G.; Gamurari, V. Ia. *Mol. Phys.* **1997**, *3*, 465.
(9) Creutz, C.; Taube, H. *J. Am. Chem. Soc.* **1969**, *91*, 3988.
(10) Robin, M. B.; Day, P. *Adv. Inorg. Chem. Radiochem.* **1967**, *10*, 247.
(11) (a) Marcus, R. A. *Discuss. Faraday Soc.* **1960**, *29*, 21. (b) Marcus, R. A.; Sutin, N. *Comments Inorg. Chem.* **1986**, *5*, 119.

and the intensity of the CT transition is related to the electronic coupling element H_{ab}:

$$H_{ab} = \frac{0.0206}{R}(\nu_{max}\epsilon_{max}\nu_{1/2})^{1/2} \quad (2)$$

Here, R (in Å) is the effective separation distance between the donor and acceptor sites (diabatic states), ϵ (in M^{-1} cm^{-1}) is the molar extinction coefficient, and $\nu_{1/2}$ is the full-width at half-maximum (with H_{ab}, ν_{max}, and $\nu_{1/2}$ in cm^{-1}). Note, that, while the parameters ϵ, ν_{max}, and $\nu_{1/2}$ are accessible from optical measurements, the diabatic transfer distance R cannot, in principle, be directly measured. Only significantly later, after the seminal work of Hush, did Cave and Newton[6c] develop a prescription on how to obtain R using experimental and/or theoretical data. We will pay special attention to this problem in the following sections.

The Hush model remains the most preferred method of analysis of the CT spectra because of its simplicity and its ease of application. This model, however, becomes inapplicable when dealing with systems that are intermediate between class II and class III. The problem arises from the failure of the Born−Oppenheimer approximation when both electronic and vibronic couplings are strong. The concept of potential energy surfaces then loses its meaning, and the CT transition can no longer be interpreted as a transition between two potential surfaces. This limitation can only be overcome in the framework of a dynamic vibronic model.[13,14]

The interest in pure organic MV systems is currently increasing.[15−22] Many of these systems, such as those recently synthesized and investigated by Lambert and Nöll,[17] display a significant electronic coupling and are intermediate between class II and class III or even belong to class III. Because a strong electronic interaction generally yields a transfer rate much faster than the typical time scale of many experimental techniques such as ESR or NMR, the CT band measurements remain one of the main experimental tools for the investigation of organic intramolecular ET processes. As a result, the development of an adequate theoretical framework to describe the CT transitions in organic MV systems constitutes an important issue.

In recent work,[22] we have shown that the dynamic vibronic model, worked out for inorganic MV systems in combination with DFT calculations, is a valuable approach as well for the study of the ET properties of organic MV systems. In the present work, this method is further developed by including both diagonal and nondiagonal vibronic interactions. This approach is applied to study the dependence of the intervalence CT transitions on bridge length (and, consequently, on the strength of electron coupling) in Lambert and Nöll[17] triarylamine-based MV systems; see Figure 1. The CT bands in these compounds are intense and well separated from other bands; thus, these systems are very suitable for accurate spectral measurements and the validation of theoretical models. We also note that triarylamine derivatives are currently widely used as hole-transport components in multilayer organic light-emitting diodes.[23−24] Therefore, the understanding of the intramolecular ET characteristics is important for the design of new materials for organic optoelectronic devices.

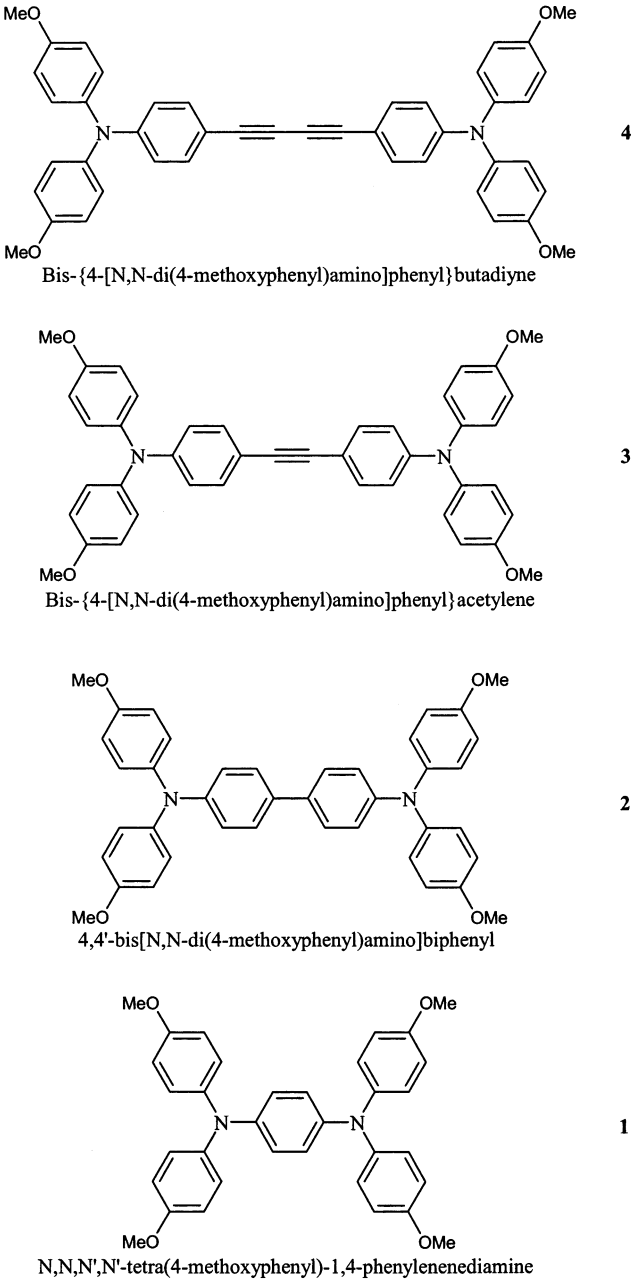

Figure 1. Chemical structure of molecules **1**−**4**.

(12) (a) Hush, N. S. *Prog. Inorg. Chem*. **1967**, *8*, 391. (b) Hush, N. S. *Coord. Chem. Rev*. **1985**, *64*, 135.
(13) (a) Piepho, S. B.; Krausz, E. R.; Schatz, P. N. *J. Am. Chem. Soc*. **1978**, *100*, 2996. (b) Wong, K. Y.; Schatz, P. N. *Prog. Inorg. Chem*. **1981**, *28*, 369.
(14) (a) Piepho, S. B. *J. Am. Chem. Soc*. **1988**, *110*, 6319. (b) Piepho, S. B. *J. Am. Chem. Soc*. **1990**, *112*, 4197.
(15) (a) Lahlil, K.; Moradpour, A.; Bowlas, C.; Menou, F.; Cassoux, P.; Bonvoisin, J.; Launay, J.-P.; Dive, G.; Dehareng, D. *J. Am. Chem. Soc*. **1995**, *117*, 9995. (b) Bonvoisin, J.; Launay, J.-P.; Verbouwe, W.; van der Auweraer, M.; De Schryver, F. C. *J. Phys. Chem*. **1996**, *100*, 17079.
(16) (a) Nelsen, S. F.; Ismagilov, R. F.; Trieber, D. A. *Science* **1997**, *278*, 846. (b) Nelsen, S. F.; Ramm, M. T.; Wolff, J. J.; Powell, D. R. *J. Am. Chem. Soc*. **1997**, *119*, 6863. (c) Nelsen, S. F.; Trieber, D. A.; Wolff, J. J.; Powell, D. R.; Rogers-Crowley, S. *J. Am. Chem. Soc*. **1997**, *119*, 6873. (d) Nelsen, S. F.; Ismagilov, R. F.; Teki, Y. *J. Am. Chem. Soc*. **1998**, *120*, 2200. (e) Nelsen, S. F. *Chem.-Eur. J*. **2000**, *6*, 581.
(17) (a) Lambert, C.; Nöll, G. *Angew. Chem., Int. Ed*. **1998**, *37*, 2107. (b) Lambert, C.; Nöll, G. *J. Am. Chem. Soc*. **1999**, *121*, 8434.
(18) Lindeman, S. V.; Rosokha, S. V.; Sun, D.; Kochi, J. K. *J. Am. Chem. Soc*. **2002**, *124*, 843.
(19) Nelsen, S. F.; Newton, M. D. *J. Phys. Chem. A* **2000**, *104*, 10023.
(20) Johnson, R. C.; Hupp, J. T. *J. Am. Chem. Soc*. **2001**, *123*, 2053.
(21) Dehareng, D.; Dive, G.; Moradpour, A. *Int. J. Quantum Chem*. **2000**, *76*, 552.
(22) Coropceanu, V.; Malagoli, M.; André, J. M.; Brédas, J. L. *J. Chem. Phys*. **2001**, *115*, 10409.

II. Vibronic Model

The first vibronic coupling model that is applicable to both class II and class III MV systems is the PKS (Piepho, Krausz, and Schatz)[13] model. It is a two-site one-mode model in which only the donor and acceptor states are considered. The vibrational mode in the PKS model represents the out-of-phase linear combination of breathing modes localized on donor and acceptor sites. Ondrechen and co-workers[25] extended this model by explicitly accounting for the role of the bridge ligand and its vibrational modes. Piepho[14] further advanced the understanding of mixed-valence systems by formulating a model that stresses the role of multicenter vibrations that govern the donor−acceptor distance. In this work, Piepho's model is applied for the investigation of the charge-transfer bands in triarylamine MV systems.

The molecular Hamiltonian can be written as

$$\mathrm{H} = \mathrm{H_e} + T_\mathrm{Q} + V(r,Q) \tag{3}$$

Here, $\mathrm{H_e}$ is the pure electronic part that includes the kinetic energy of electrons and the interelectronic electrostatic interactions; T_Q is the kinetic energy of the nuclei; and $V(r,Q)$ is the operator for electron−nuclear interactions and internuclear repulsions; r, Q are standard notations for electronic and nuclear coordinates, respectively. As is customary in the vibronic problem of molecules,[26] we choose the symmetric nuclear configuration of the molecule as the reference geometry ($Q_0 = 0$). The function $V(r,Q)$ is then expanded with respect to small nuclear displacements around the reference point. In the harmonic approximation and using the normal coordinates Q_α, the operator $V(r,Q)$ can be expressed as

$$V(r,Q) = V(r,Q_0) + \sum_\alpha \left(\frac{\partial V}{\partial Q_\alpha}\right)_{Q_0} Q_\alpha + {}^1/_2 \sum_{\alpha\beta} \left(\frac{\partial^2 V}{\partial Q_\alpha \partial Q_\beta}\right)_{Q_0} Q_\alpha Q_\beta \tag{4}$$

The eigenfunctions $\Phi_i(r,Q)$ of the complete Hamiltonian can be sought in the form:

$$\Phi_i(r,Q) = \sum_j \eta_{ij}(Q)\Psi_j(r,Q_0) \tag{5}$$

where the electronic wave functions $\Psi(r,Q_0)$ are the eigenfunctions of the electronic Hamiltonian with the fixed nuclear coordinates at the reference geometry:

$$[\mathrm{H_e} + V(r,Q_0)]\Psi_j(r) = \epsilon_j \Psi_j(\mathrm{r}) \tag{6}$$

As we show below, only two electronic states $\Psi_+(r)$ (symmetric) and $\Psi_-(r)$ (antisymmetric) with energy ϵ_+ and ϵ_-, respectively, are involved in the CT transition for all of the systems considered here. Therefore, for the sake of simplicity, we limit the electronic basis set to a two-state model. These states can mix significantly through vibronic interactions even if they are not vibronically coupled to other excited states.

The linear vibronic interaction (the only one considered here) is defined by the matrix elements of the second term in eq 4:

$$l_\alpha^i = \langle \Psi_i | \partial V/\partial Q_\alpha | \Psi_i \rangle \tag{7}$$

$$l_\alpha^{ij} = \langle \Psi_i | \partial V/\partial Q_\alpha | \Psi_j \rangle \tag{8}$$

$l_\alpha{}^i$ and $l_\alpha{}^{ij}$ are known as the diagonal and off-diagonal linear vibronic constants,[26] respectively. From the selection rules, it follows that the off-diagonal vibronic coupling is determined by antisymmetric vibrations only, while the diagonal vibronic coupling is entirely determined by the totally symmetric vibrations. Following Piepho,[14] we hereafter consider a simple two-mode vibronic model, containing only the contributions of one symmetric vibration Q_+ and one antisymmetric vibration Q_-. In this approximation, the expansion coefficients $\eta_{ij}(Q)$ can be determined by solving the following vibronic matrix $\mathrm{H_{vib}}$:

$$\mathrm{H_{vib}} = \begin{pmatrix} T_{Q+} + T_{Q-} + \frac{1}{2}(k_- Q_-^2 + k_+ Q_+^2) & l_- Q_- \\ l_- Q_- & T_{Q+} + T_{Q-} + \frac{1}{2}(k_- Q_-^2 + k_+ Q_+^2) + \Delta + l_+ Q_+ \end{pmatrix} \tag{9}$$

Here, k_+ and k_- are the force constants, and we assume that they are the same in both electronic states Ψ_+ and Ψ_-; l_+ and l_- are the diagonal and off-diagonal linear vibronic constants, respectively. The energy difference between the molecular electronic states $\Psi_\pm$, $\Delta = \epsilon_+ - \epsilon_-$, is related to the electronic coupling constant $\mathrm{H_{ab}}$ by

$$\Delta = 2\mathrm{H_{ab}} \tag{10}$$

The eigenvalues and eigenfunctions of the vibronic matrix $\mathrm{H_{vib}}$ form the complete solution of the dynamic vibronic problem.

1. Off-Diagonal Vibronic Constant. To shed more light on the physical meaning of the vibronic constants, we first consider the static (adiabatic) solutions of the problem, that is, the solutions obtained in the framework of the Born−Oppenheimer approximation from the electronic Hamiltonian only, without considering the nuclear kinetic energy. We first consider the case where only the off-diagonal vibronic coupling is operative, that is, $l_- \neq 0$ and $l_+ = 0$. The adiabatic potential surfaces we obtained are plotted in Figure 2. Provided $l_-{}^2/k_- > \mathrm{H_{ab}}$ (class II), the vibronic mixing of different electronic states leads to a pseudo-Jahn−Teller instability of the reference symmetric geometry; the lower surface of the adiabatic potential exhibits two equivalent minima corresponding to two broken-symmetry states. Each of these minima corresponds to the situation where the system is mainly localized on one of the valence structures $\mathrm{M_a{}^+-L_{\mathit{i}}-M_b}$ or $\mathrm{M_a-L_{\mathit{i}}-M_b{}^+}$. Thus, the vibration Q_- (pseudo-Jahn−Teller mode) corresponds to the reaction coordinate of the standard one-dimensional self-exchange ET theory.[11] The

(23) (a) Bulovic, V.; Gu, G.; Burrows, P. E.; Forrest, S. R.; Thompson, M. E. *Nature* **1996**, *380*, 29. (b) Tamoto, N.; Adachi, C.; Nagai, K. *Chem. Mater.* **1997**, *9*, 1077. (c) Bellmann, E.; Shaheen, S. E.; Thayumanavan, S.; Barlow, S.; Grubbs, R. H.; Marder, S. R.; Kippelen, B.; Peyghambarian, N. *Chem. Mater.* **1998**, *10*, 1668. (d) Bellmann, E.; Shaheen, S. E.; Grubbs, R. H.; Marder, S. R.; Kippelen, B.; Peyghambarian, N. *Chem. Mater.* **1999**, *11*, 399.

(24) Cornil, J.; Gruhn, N. E.; dos Santos, D. A.; Malagoli, M.; Lee, P. A.; Barlow, S.; Thayumanavan, S.; Marder, S. R.; Armstrong, N. R.; Brédas, J. L. *J. Phys. Chem. A* **2001**, *105*, 5206.

(25) (a) Root, L. J.; Ondrechen, M. J. *Chem. Phys. Lett.* **1982**, *93*, 421. (b) Ko, J.; Ondrechen, M. J. *Chem. Phys. Lett.* **1984**, *112*, 507. (c) Ko, J.; Ondrechen, M. J. *J. Am. Chem. Soc.* **1985**, *107*, 6161. (d) Ondrechen, M. J.; Ko, J.; Zhang, L.-T. *J. Am. Chem. Soc.* **1987**, *109*, 1672.

(26) Bersuker, I. B. *The Jahn−Teller Effect and Vibronic Interactions in Modern Chemistry*; Plenum Press: New York, 1984.

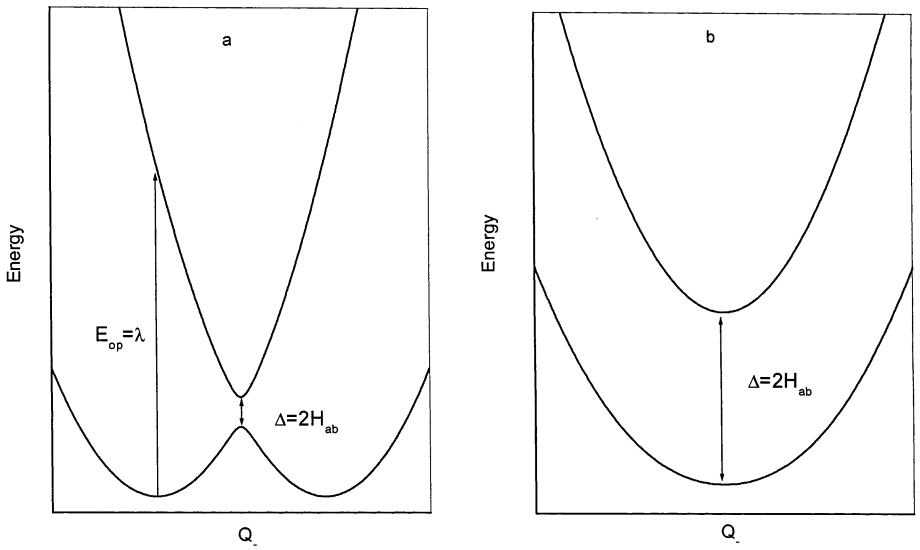

Figure 2. Sketch of typical adiabatic energy surfaces in the case of off-diagonal vibronic coupling: (a) class-II system; (b) class-III system.

vibronic constant is related to the Marcus reorganization energy λ by

$$\lambda = 2l_-^2/k_- \tag{11}$$

When $l_-^2/k_- \leq H_{ab}$ (class III), the lower surface possesses only one minimum, and the symmetric equilibrium structure is then stable with respect to the antisymmetric vibrations.

The optical transfer, due to the Franck−Condon principle, is a vertical transition from a minimum in the lower surface to the upper surface; see Figure 2. In the case of weakly coupled systems ($H_{ab} < l_-^2/k_-$ or equivalent $\Delta < \lambda$), the maximum of the CT band is independent[4c,6b] of H_{ab} and is given by eq 1. The CT band is Gaussian-shaped with a full-width at half-maximum given at high temperatures by the Hush relation:[12]

$$\nu_{1/2}^2 = 16\lambda k_B T \ln 2 \tag{12}$$

where k_B is the Boltzmann constant. An increase in electronic coupling generally results in a more intense asymmetric and narrower band. In the case of strongly coupled MV systems, $\Delta > \lambda$ (class III), the energy of the intervalence transition becomes a direct measure of the electronic coupling:

$$E_{op} = \Delta = 2H_{ab} \tag{13}$$

In the present context, the CT transition dipole moment μ_{12} is a quantity of interest. By making use of the explicit form of the electronic eigenfunctions associated with the adiabatic potential surfaces[13] (static solutions, that is, the eigenfunctions obtained from the vibronic Hamiltonian (eq 9) only, without considering the nuclear kinetic energy):[27]

$$\Psi_1 = N\{-(H_{ab} - \sqrt{H_{ab}^2 + l_-^2 Q_-^2})\Psi_+ + l_- Q_- \Psi_-\} \tag{14}$$

$$\Psi_2 = N\{l_- Q_- \Psi_+ + (H_{ab} - \sqrt{H_{ab}^2 + l_-^2 Q_-^2})\Psi_-\} \tag{15}$$

$$N = ((H_{ab} - \sqrt{H_{ab}^2 + l_-^2 Q_-^2})^2 + l_-^2 Q_-^2)^{-1/2} \tag{16}$$

we obtain

$$|\mu_{12}| = \begin{cases} \dfrac{\Delta}{\lambda}|\mu_\pm| & \text{for } \Delta < \lambda \\ |\mu_\pm| & \text{for } \Delta \geq \lambda \end{cases} \tag{17}$$

where $\mu_\pm$ is the transition dipole moment for the electronic $\Psi_+ \rightarrow \Psi_-$ transition. The latter equation clearly shows that there is a direct relationship between the degree of localization−delocalization measured by Δ/λ and the intensity of the CT transition. The transition dipole moment $\mu_\pm$ can be straightforwardly calculated by expanding the molecular electronic states Ψ_+ and Ψ_- into the localized states Ψ_a and Ψ_b:

$$\Psi_\pm = \frac{1}{\sqrt{2}}(\Psi_a \pm \Psi_b) \tag{18}$$

It results that $\mu_\pm$ is parallel to the ET vector and thus the CT transition is polarized accordingly. Its magnitude is related to the ET distance, R, by[13]

$$|\mu_\pm| = |eR/2| \tag{19}$$

Introducing eqs 1, 10, and 19 into eq 17, we obtain

$$H_{ab} = \frac{\mu_{12}}{eR} E_{op} \tag{20}$$

For the particular case of Gaussian-shaped CT bands, eq 20 leads to eq 2.

The latter equation and the equivalent eq 2 have been initially derived at the perturbation limit of weak electronic coupling. Creutz and co-workers[6b] showed that this equation is exact within the two-state model. This finding led to the widely accepted conclusion that eq 20 is applicable for all systems ranging from those that are very weakly coupled to those that are very strongly coupled. *We emphasize, however, that eq 20 has been derived from static solutions and is applicable only when these solutions are valid. In general, one has to solve the dynamic vibronic problem.*

Generally, the concept of adiabatic potential and the corresponding eigenfunctions are valid in the case of strongly coupled systems ($\Delta \gg \hbar\omega_-$, where $\hbar\omega_-$ is the energy of vibrational

(27) Solutions Ψ_1 and Ψ_2 correspond to the lower and upper adiabatic surfaces, respectively (Figure 2a). At the symmetric nuclear configuration, Ψ_1 merges to Ψ_+ or Ψ_- depending on whether the transfer integral H_{ab} is negative or positive, respectively (because at $Q_- = 0$, the treatment of general solutions (eqs 14−16) requires special care, it is more convenient to obtain Ψ_1 and Ψ_2 by solving eq 9 for $Q_- = 0$ separately).

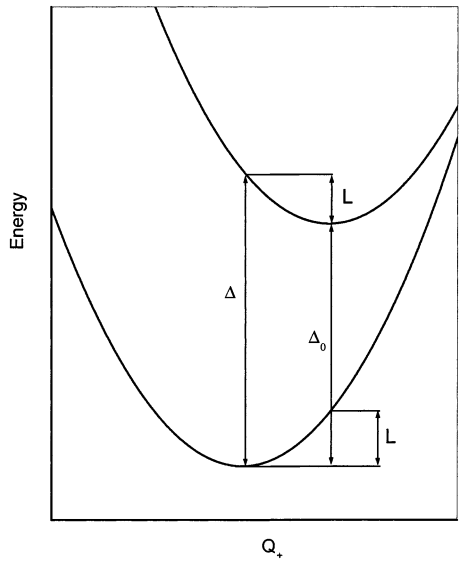

Figure 3. Sketch of a typical adiabatic energy surface in the case of diagonal vibronic coupling.

mode Q_-); the energy gap between the two adiabatic potential (AP) surfaces is then sufficiently large, precluding their interaction. However, because the CT transitions are determined by the system wave functions taken at the nuclear configurations of the minima of the lowest potential surface, the CT transitions can be described within the framework of the adiabatic approximation as well in the case of very strong vibronic interactions $\lambda \gg \Delta$ (strong pseudo-Jahn−Teller effect) even for weak electronic coupling.

2. Diagonal Vibronic Constant. We now consider the case where only the diagonal vibronic coupling is taken into account, $l_+ \neq 0$ and $l_- = 0$. The diagonal vibronic coupling results in a displacement of the upper surface with respect to the ground AP surface. The corresponding AP surfaces are shown in Figure 3. This displacement is due to the sensitivity of the molecular geometry to the change in electron distribution occurring during the optical excitation. This means that in a Franck−Condon transition the molecule undergoes a change of both its electronic and its symmetrical vibrational states. Thus, the energy of the intervalence transition can be written as

$$E_{op} = \Delta = \Delta_0 + L; \quad L = k_+(\delta Q_+)^2/2 \tag{21}$$

where Δ_0 is the energy difference between the ground and excited states each at their own equilibrium positions, and $\delta Q_+ = l_+/k_+$ is the displacement of the two AP curves. In the conventional molecular spectroscopy, the quantity L is usually referred to as the relaxation energy. Note, however, that both quantities λ and L bear the same physical meaning (that is, the vibrational reorganization energy) and are being distinguished only by the relevant vibrational mode (that is, antisymmetric or symmetric). The band shape is directly related to the dimensionless quantity $S_+ = L/\hbar\omega_+$ ($\hbar\omega_+$ is the energy of vibrational mode Q_+), the Huang−Rhys factor; it is numerically equal to the number of vibrational quanta involved in the CT transition. For significant diagonal vibronic coupling, the CT band at high temperatures is Gaussian-shaped,[26] as in the case of strong off-diagonal vibronic coupling. Moreover, the full-width at half-maximum is given by the same relation, that is, eq 12, in which parameter λ is replaced by L:

$$\nu_{1/2}^2 = 16Lk_BT \ln 2 \tag{22}$$

Thus, if the interaction with symmetric vibrations is strong, the shape of the CT band can be broad even in the case of class III systems. Therefore, the shape of the CT band alone is generally not a good measure of the strength of the electronic coupling.

Interestingly, the fact that the interaction with symmetric vibrations could be a major source of band broadening for strongly delocalized MV systems has been predicted as well by Hush.[28] This prediction has been later confirmed for the Creutz−Taube ion[14] and the MV iron $[Fe_2(OH)_3(tmtacn)_2]^{2+}$ compound.[29] Here, we show that symmetric vibrations play an even greater role in delocalized MV organic systems.

3. Dynamic Solution. The full dynamic solution of the vibronic Hamiltonian given by eq 9 can be obtained only numerically, by expanding the coefficients $\eta_{ij}(Q)$ in eq 5 in terms of a complete orthonormal set. It is more convenient to use the harmonic oscillator functions $\chi_n(Q)$:

$$\Phi_i(r,Q) = \Psi_+ \sum_{nm} c_{inm}^+ \chi_n(Q_+)\chi_m(Q_-) + \Psi_- \sum_{nm} c_{inm}^- \chi_n(Q_+)\chi_m(Q_-) \tag{23}$$

On this basis, the solution of the dynamic problem is transformed into an eigenvalue problem of an infinite set of linear equations (see details in ref 14a). However, by limiting the total number of vibrational quanta in this expansion (eq 23) to a finite but large value, one can obtain the solutions of the dynamic vibronic problem with any arbitrary accuracy.

In this case, the transition dipole moment (transition vibronic moment) between the vibronic states $\Phi_i(r,Q)$ and $\Phi_j(r,Q)$ is given by

$$\mu_{ij} = \mu_\pm M(c_i,c_j) \tag{24}$$

The quantity $M(c_i,c_j)$ depends only on the expansion coefficients c_i of the corresponding vibronic states and plays a role similar to that of the parameter Δ/λ in adiabatic calculations (see eq 17). The transition vibronic moments (whose values we do not explicitly provide) and the eigenvalues of the dynamic matrix are used below to simulate the shape and intensity (the oscillator strengths) of the CT bands. The electronic parameters are derived from electronic-structure calculations; our choice for the other parameters that enter into the dynamic matrix is discussed in the following sections.

III. Electronic Structure Calculations

1. Computational Methodology. The geometry of the molecules shown in Figure 1 has been optimized for three different electronic configurations, corresponding to the neutral system, the radical-cation in the ground state, and the radical-cation in the first excited state. Because we are interested in the location of the symmetric geometry configuration (reference

(28) (a) Hush, N. S., in ref 2. (b) Reimers, R.; Hush, N. S. *Chem. Phys.* **1996**, *208*, 177.
(29) Gamelin, D. R.; Bominaar, E. L.; Mathoniere, C.; Kirk, M. L.; Weighardt, K.; Girerd, J.-J.; Solomon, E. I. *Inorg. Chem.* **1996**, *35*, 4323.

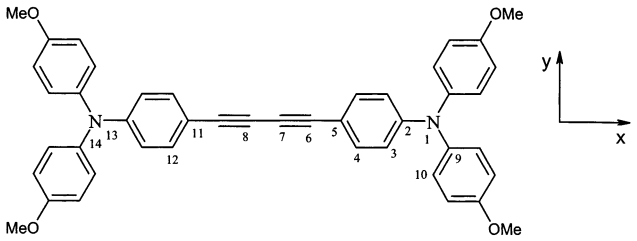

Figure 4. Chemical structure of the *N*,*N*,*N*′,*N*′-tetrakis(4-methoxyphenyl)-1,4-benzenediamine molecule (**4**) with atom labeling and description of the reference system.

configuration), the optimization of the radical-cation states has been performed with symmetry constraints, that is, keeping the two halves of the molecule identical. Geometry optimizations with relaxed symmetry constraints have also been performed. The calculations were carried out at the DFT level, using the B3LYP functional, where Becke's three-parameter hybrid exchange functional is combined with the Lee−Yang−Parr correlation functional.[30,31]

The excitation energies and transition dipole moments of the low-lying excited states have been calculated at the TD-DFT level.[32] In this method, the dynamic response of the charge density for a system, exposed to a time-dependent perturbation, is described by a time-dependent Kohn−Sham-like equation. The poles and residues of the dynamic polarizability correspond to the vertical excitation energies and oscillator strengths, respectively. The same B3LYP functional was used in all TD-DFT calculations. In addition, we have also performed ab initio spin-restricted Hartree−Fock (HF) calculations on the spin-singlet state of the neutral systems; the results were used to estimate the electronic coupling constants in the framework of Koopmans' theorem (KT). All DFT and ab initio calculations were carried out with the 6-31G** split valence plus polarization basis set,[33] using the Gaussian 98 suite of programs.[34]

2. Geometry. The main results of the geometry optimizations on the neutral, radical-cation ground-state, and radical-cation excited-state geometries for systems **1**−**4** (using the labels of Figure 4) are collected in Table 1. In the present study, we are mainly concerned with the geometry relaxations due to two different electronic processes: (i) the formation of the radical-cation and (ii) the electronic excitation of the radical-cation. Previous theoretical investigations of bis-triarylamine systems have indicated that, when the electronic structure is changed from the neutral to the radical-cation state, the largest geometry relaxation occurs in the conjugated bridge connecting the two nitrogen atoms.[22,35] These findings are confirmed by the present results, which further show that the relaxation connected with the electronic excitation of the cation state is also mainly localized on the bridge. For these reasons, our discussion of the geometrical changes is focused on the central segment of the systems.

When going from the neutral system to the radical-cation, the geometry modifications are consistent through the series **1**−**4**; we observe a shortening of the central C−N bond and an increase in the quinoidic character of the central phenylene rings. In the systems containing triple C−C bonds, $\mathbf{3}^+$ and $\mathbf{4}^+$, the length of the triple bond is slightly increased, while the central single bonds slightly shorten. The four radical-cations are characterized also by a decrease in the twist angle between the central phenylene rings and the amino groups. In $\mathbf{2}^+$, the twist angle between the two central rings also decreases.

With regard to the relaxations taking place upon excitation of the cations, we note a considerable increase in the C−N bond length, while the remaining bond lengths of the central bridge reverse back to values very similar to those found in the corresponding neutral system. The largest C−N relaxation occurs in the smallest system $\mathbf{1}^{+}$***** (0.044 Å, see Table 1); the corresponding values in $\mathbf{2}^{+}$*****, $\mathbf{3}^{+}$*****, and $\mathbf{4}^{+}$***** are 0.033, 0.031, and 0.028 Å, respectively. All of the excited states are characterized by a sharp increase in the dihedral twist angle between the planes of the two amino groups, as can be seen by inspection of the last row of Table 1.

Table 1 also collects the N−N distance for all of the systems studied. In a way, consistent with the modifications in the central bridge, the N−N separations are shorter in the ground state of the cations, while the neutral systems and the cation excited states have similar higher values. In contrast to the C−N relaxation, the magnitudes of the relaxations of the N−N distances increase on going from **1** to **4**.

3. Electronic Coupling. In the present work, the Δ value, and thus the electronic coupling parameter, is evaluated in three ways: (a) from the energy spectrum obtained at the TD-DFT level; (b) directly from DFT calculations; and (c) by means of Koopmans' theorem.[36] As seen from Figure 2, in class-II compounds, the coupling parameter Δ should be calculated at the transition-state structure rather than at the equilibrium geometry. To rule out a possible artifact of the DFT geometry optimizations in the case of the radical-cation, as a crosscheck, all of the electronic calculations have been also carried out at the neutral molecular geometry; the latter is actually used in many practical studies as a first approximation to the transition-state geometry.[6a]

The TD-DFT energy and transition dipole moment of the first excited state of systems $\mathbf{1}^{+}$−$\mathbf{4}^{+}$ are given in Table 2. The results indicate that the first optical band is due to a single electronic transition to an excited state well separated from any other state. For all four systems, the main configuration interaction (CI) contribution to the state in question is described by the HOMOβ → LUMOβ one-electron transition (if we were to use the labels of the levels in the neutral state, this would correspond to the HOMO−1 → HOMO excitation). The contour plots of the

(30) (a) Becke, A. D. *Phys. Rev. A* **1988**, *38*, 3098. (b) Becke, A. D. *J. Chem. Phys.* **1993**, *98*, 5648.
(31) Lee, C.; Yang, W.; Parr, R. G. *Phys. Rev. B* **1988**, *37*, 785.
(32) (a) Casida, M. E.; Jamorski, C.; Casida, K. C.; Salahub, D. R. *J. Chem. Phys.* **1998**, *108*, 4439. (b) Stratmann, R. E.; Scuseria, G. E.; Frisch, M. J. *J. Chem. Phys.* **1998**, *109*, 8218.
(33) (a) Ditchfield, R.; Hehre, W. J.; Pople, J. A. *J. Chem. Phys.* **1971**, *54*, 724. (b) Hehre, W. J.; Ditchfield, R.; Pople, J. A. *J. Chem. Phys.* **1972**, *56*, 2257. (c) Hariharan, P. C.; Pople, J. A. *Mol. Phys.* **1974**, *27*, 209. (d) Gordon, M. S. *Chem. Phys. Lett.* **1980**, *76*, 163. (e) Hariharan, P. C.; Pople, J. A. *Theor. Chim. Acta* **1973**, *28*, 213.
(34) Frisch, M. J.; Trucks, G. W.; Schlegel, H. B.; Scuseria, G. E.; Robb, M. A.; Cheeseman, J. R.; Zakrzewski, V. G.; Montgomery, J. A., Jr.; Stratmann, R. E.; Burant, J. C.; Dapprich, S.; Millam, J. M.; Daniels, A. D.; Kudin, K. N.; Strain, M. C.; Farkas, O.; Tomasi, J.; Barone, V.; Cossi, M.; Cammi, R.; Mennucci, B.; Pomelli, C.; Adamo, C.; Clifford, S.; Ochterski, J.; Petersson, G. A.; Ayala, P. Y.; Cui, Q.; Morokuma, K.; Malick, D. K.; Rabuck, A. D.; Raghavachari, K.; Foresman, J. B.; Cioslowski, J.; Ortiz, J. V.; Baboul, A. G.; Stefanov, B. B.; Liu, G.; Liashenko, A.; Piskorz, P.; Komaromi, I.; Gomperts, R.; Martin, R. L.; Fox, D. J.; Keith, T.; Al-Laham, M. A.; Peng, C. Y.; Nanayakkara, A.; Challacombe, M.; Gill, P. M. W.; Johnson, B.; Chen, W.; Wong, M. W.; Andres, J. L.; Gonzalez, C.; Head-Gordon, M.; Replogle, E. S.; Pople, J. A. *Gaussian 98*, revision A.9; Gaussian, Inc.: Pittsburgh, PA, 1998.
(35) Malagoli, M.; Brédas, J. L. *Chem. Phys. Lett.* **2000**, *327*, 13.
(36) Koopmans, T. *Physica* **1933**, *1*, 104.

Table 1. Selected Geometrical Parameters, Computed at the DFT B3LYP/6-31G** Level, for the Four Molecules Studied in the Present Work[a]

	1	**1**$^+$	**1**$^{+*}$	**2**	**2**$^+$	**2**$^{+*}$	**3**	**3**$^+$	**3**$^{+*}$	**4**	**4**$^+$	**4**$^{+*}$
						Bond Length (Å)						
N_1-C_2	1.418	1.390	1.434	1.413	1.393	1.426	1.411	1.391	1.422	1.408	1.390	1.418
C_2-C_3	1.405	1.418	1.400	1.406	1.416	1.402	1.408	1.418	1.405	1.409	1.419	1.407
C_3-C_4	1.390	1.378	1.393	1.390	1.380	1.391	1.388	1.378	1.388	1.387	1.378	1.367
C_4-C_5				1.406	1.416	1.405	1.410	1.419	1.410	1.411	1.420	1.411
C_5-C_6				1.480	1.459	1.487	1.421	1.403	1.425	1.418	1.400	1.421
C_6-C_7							1.218	1.225	1.216	1.223	1.231	1.221
C_7-C_8										1.358	1.344	1.361
N_1-N_{13}	5.676	5.621	5.671	10.005	9.949	9.987	12.564	12.485	12.550	15.136	15.055	15.123
						Dihedral Angle (deg)						
$C_3C_2N_1C_9$	37	29	54	32	27	47	33	29	43	31	28	40
$C_{10}C_9N_1C_2$	45	46	35	48	48	38	47	48	39	48	48	40
$C_{12}C_{11}C_5C_4$				36	25	39	1	1	3	4	1	1
$C_{14}N_{13}N_1C_9$	74	58	106	29	29	55	65	58	83	65	54	80

[a] For each system, three electronic configurations are considered: the neutral state, the radical-cation ground state, and the radical-cation lowest excited state (the atom labeling is shown in Figure 4).

Table 2. TD-DFT Vertical Excitation Energy Δ, Transition Dipole Moment $\mu_{\pm}$, and Configuration Description of the Lowest Excited State of Systems **1**$^+$−**4**$^+$ Obtained at the Radical-Cation Geometry and, between Parentheses, at the Neutral State Geometry

	Δ [cm^{-1}]			transition dipole moment [D][b] $\mu_{\pm}$		configuration descriptions and weights			E_{op} [cm^{-1}][c]	μ_{exp} [D][c]
1$^+$	9250	(7940)	η[a] = 1.16	10.13	(10.50)	HOMO α → LUMO+1 α	0.16	(0.13)	9530	9.17
						HOMO β → LUMO β	0.87	(0.82)		
2$^+$	6920	(5860)	η = 1.18	14.52	(14.67)	HOMO α → LUMO α	0.18	(−0.14)	6360	11.6
						HOMO β → LUMO β	0.78	(0.72)		
3$^+$	6550	(5900)	η = 1.11	16.55	(16.82)	HOMO α → LUMO α	0.21	(0.17)	6190	11.6
						HOMO β → LUMO β	0.77	(0.72)		
4$^+$	6040	(5480)	η = 1.10	18.53	(18.82)	HOMO α → LUMO α	0.21	(−0.18)	7550	6.39
						HOMO β → LUMO β	0.76	(0.70)		

[a] η = Δ(at cation geometry)/Δ(at neutral geometry). [b] Only the absolute value of the transition dipole component parallel to the NN axis is shown; the other two components are equal to zero or negligibly small. [c] The experimental data (obtained in CH_2Cl_2) are taken from ref 17.

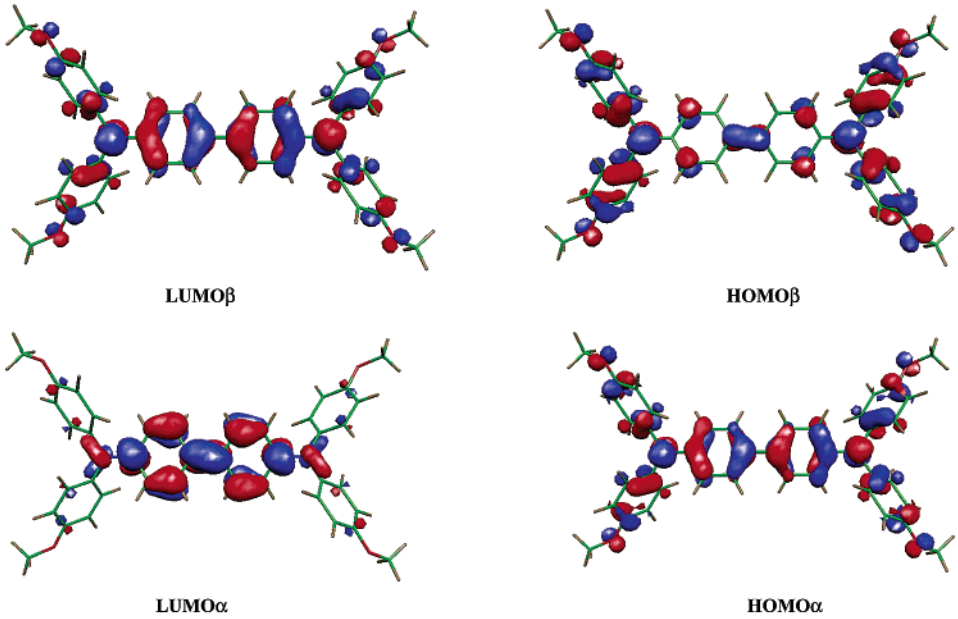

Figure 5. Contour plots of the HOMOβ, LUMOβ, HOMOα, and LUMOα molecular orbitals of **2**$^+$, as obtained at the DFT/6-31G** level.

corresponding orbitals for systems **2**$^+$ and **4**$^+$ are shown in Figures 5 and 6, respectively. As can be deduced from these figures, the HOMO β and LUMO β orbitals of each system (as well as those of systems **1**$^+$ and **3**$^+$) are of opposite parity; each basically represents a symmetry combination (with respect to the symmetry plane perpendicular to the NN axis) of the two orbital portions localized on the different halves of the molecules. Besides this main contribution, the lowest excited state of all cations has contributions from the HOMOα → LUMOα (see Figures 5 and 6) transition for systems **2**$^+$, **3**$^+$, and **4**$^+$ and the HOMOα → LUMO+1α transition for cation **1**$^+$; the calculations indicate that the weight of the higher-excited configurations slightly increases as the bridge is elongated.

In the case of open-shell molecules, the DFT method can be used directly to calculate the lowest state of any symmetry. Because in our case the two states of interest, Ψ_+ and Ψ_-, are

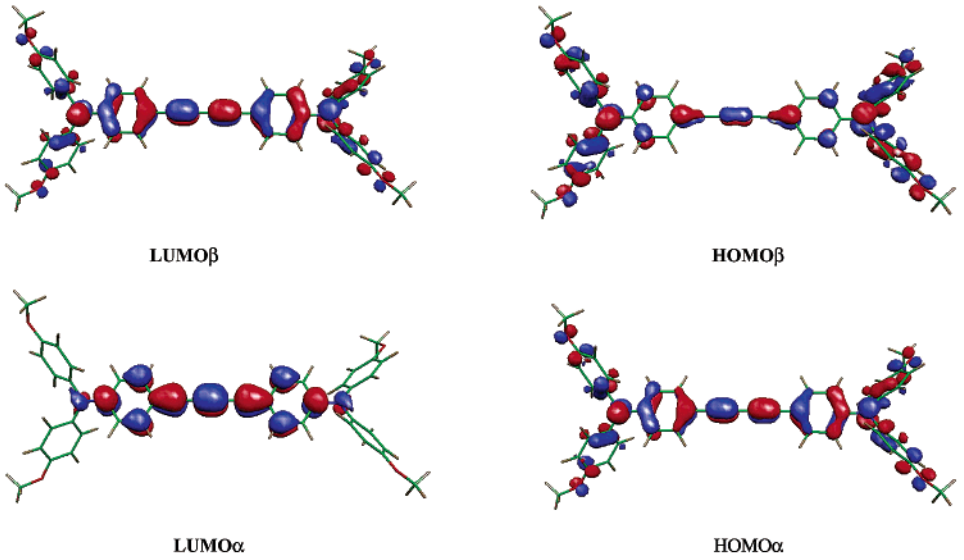

Figure 6. Contour plots of the HOMOβ, LUMOβ, HOMOα, and LUMOα molecular orbitals of $\mathbf{4}^+$, as obtained at the DFT/6-31G** level.

Table 3. Absolute Values of Parameter Δ (in cm^{-1}) for Systems $\mathbf{1}^+$−$\mathbf{4}^+$ Obtained from DFT and KT Calculations Using the Geometry of the Radical-Cation State and, between Parentheses, of the Neutral State

method/system	$\mathbf{1}^+$	$\mathbf{2}^+$	$\mathbf{3}^+$	$\mathbf{4}^+$
DFT(B3LYP/ 6-31G**)	7280	4290	3950	3640
KT (HF/ 6-31G**)[a]	9930 (7460)	7080 (5090)	6570 (5140)	5390 (4290)
η	1.33	1.39	1.28	1.26
KT (B3LYP/ 6-31G***)[a]	7720 (5720)	4660 (3310)	4550 (3540)	3970 (3160)
η	1.34	1.41	1.29	1.26
KT-AM1-RHF[a]	6850 (4740)	4190 (2820)	3460 (2510)	2650 (1970)
η	1.45	1.49	1.38	1.34
KT-AM1-RHF[b]	9490 (4860)	(2520)	(2540)	(1890)
η	1.95			

[a] Calculated from the closed-shell electronic configuration considering DFT-optimized geometries. [b] Calculated from the closed-shell electronic configuration considering AM1-optimized geometries (taken from ref 17b).

of different symmetry, it is possible to estimate the electronic coupling parameter, $\Delta = \epsilon_+ - \epsilon_-$, by applying directly the DFT method to these two states. The DFT values of Δ are given in Table 3. For all of the systems, the DFT estimates are smaller than the TD-DFT values. This result is not unexpected because it was found earlier for other symmetric MV systems that DFT underestimates the coupling constant by at least 20−30% with respect to more correlated methods.[37] As seen from Tables 2 and 3, the discrepancy between the DFT and TD-DFT estimates increases for the longer systems, likely as a consequence of the increasing mixing of configurations in the latter systems.

Currently, the evaluation of the electronic coupling is frequently based on the simple application of Koopmans' theorem.[36] In this approach, the magnitude of Δ is approximated by the energy difference between the delocalized active molecular orbitals taken from a selected electronic configuration. We have recently[22] argued that for compound $\mathbf{1}^+$, KT estimates derived from the closed-shell configuration of the neutral molecule (Δ is obtained from the difference in the energies of the HOMO and HOMO−1 levels) agree well with the TD-DFT results. We have found the same trend for the other triarylamine systems investigated here. In what follows, accordingly we only discuss the results obtained from this configuration. Both Hartree−Fock-type and Kohn−Sham-type (KS) orbitals have been used; the results, along with the AM1 results obtained by Lambert and Nöll,[17b] are collected in Table 3. The comparison of the data in Tables 2 and 3 indicates that the KT-KS values are somewhat larger than the DFT values but remain significantly lower than the TD-DFT estimates. In contrast, the KT-HF values compare reasonably well with the TD-DFT results. The Δ parameters have been previously calculated by Lambert and Nöll[17] at the KT-AM1 level, using the AM1-optimized geometry of the neutral species. Except for compound $\mathbf{1}^+$, the KT-AM1 results are much lower than the TD-DFT values. It is useful to note that the KT-AM1 results obtained using the DFT-optimized geometries of the neutral molecules match (see Table 3) the results obtained with AM1-optimized geometries very well.

To illustrate the influence of the geometry choice on the TD-DFT and KT results, we have calculated the ratio η = Δ(at cation geometry)/Δ(at neutral geometry). From the data given in Tables 2 and 3, it follows that the TD-DFT values are less sensible to the choice of geometry than are the KT estimates; the biggest TD-DFT value of η is obtained for compound $\mathbf{2}^+$, $\eta = 1.18$, and is to be compared to $\eta = 1.39$, 1.41, and 1.49 obtained for the same compound from KT-KS, KT-HF, and KT-AM1 calculations, respectively.

The aspect to emphasize is that our results indicate the presence of a significant electronic coupling in all of the investigated systems. Because the TD-DFT calculations reveal that the lowest absorption band of the $\mathbf{1}^+$−$\mathbf{4}^+$ compounds contains a single electronic excited state, the use of a two-state model is justified for the derivation of the vibronic model (eq 9).

4. Transition Dipole Moment $\mu_\pm$; Electron-Transfer Distances. In addition to excitation energies, the TD-DFT method allows for the calculation of transition dipole moments. The values of $\mu_\pm$ are collected in Table 2. It can be seen that $\mu_\pm$ is less sensitive to the geometry changes than the transition energies. The TD-DFT results indicate that only the *x*-component (the axis parallel to the bridge, see Figure 4) of $\mu_\pm$ is different of zero in the lowest absorption band. This means that the electronic transition is polarized along the NN axis, which

(37) Calzado, C. J.; Malrieu J.-P. *Chem. Phys. Lett.* **2000**, *317*, 404.

Table 4. Diabatic R and Adiabatic R_{12} ET Distances for Systems $\mathbf{1}^+-\mathbf{4}^+$ Obtained from TD-DFT Calculations

	$\mathbf{1}^+$	$\mathbf{2}^+$	$\mathbf{3}^+$	$\mathbf{4}^+$
R (Å)	4.22	6.05	6.89	7.72
R_{12} (Å)	1.79	3.64	4.92	7.24
R_{NN} (Å)[a]	5.62	9.95	12.49	15.06
R_{12}/R	0.42	0.60	0.71	0.94

[a] The nitrogen−nitrogen distances are taken from the DFT-optimized geometries of the radical-cation state.

is exactly what one would expect for a CT transition related to ET oscillations along this axis. This finding, together with the structure of the molecular orbitals (Figures 5 and 6), supports the assignment of the lowest optical transition in $\mathbf{1}^+-\mathbf{4}^+$ as a CT transition.

We stress, however, that the CT band in present systems cannot be exclusively associated to an electron-transfer process. The detailed analysis of the molecular orbitals (Figures 5 and 6) involved in the CT transition reveals that there occurs as well a shift in charge density from the terminal phenylene rings toward the central part of the molecules. We suggest that this effect can be one of the origins of the solvent dependence observed for the CT transition in all of the systems studied here.

The $\mu_\pm$ term is generally needed for the determination of the overall intensity (oscillator strength) of the CT band. Additionally, the knowledge of $\mu_\pm$ offers via eq 19 a direct possibility of estimating the electron-transfer distance R, that is, the effective separation of the diabatic (localized) states. The values of R are collected in Table 4; they indicate that the electron-transfer distance is much smaller than the nitrogen−nitrogen distance (that could, in principle, be considered as the geometric separation of the two localized sites). Another quantity widely discussed in the literature is the adiabatic ET distance R_{12}, associated with the thermal ET process between the adiabatic states.[6c,19,20] Numerically, R_{12} is related to the difference $\Delta\mu_{12}$ between the dipole moments corresponding to the minima of adiabatic potential surfaces:[6c]

$$R_{12} = |\frac{\Delta\mu_{12}}{e}| \tag{25}$$

Using the adiabatic eigenfunctions (eqs 14−16) and eqs 17−18, we obtain a useful relationship between $\Delta\mu_{12}$ and the transition dipole moments μ_{12} and $\mu_\pm$:

$$\Delta\mu_{12} = 2(\mu_\pm^2 - \mu_{12}^2)^{1/2} \tag{26}$$

Equation 26, in a different form, has been obtained originally by Cave and Newton[6c] in the framework of generalized Mulliken−Hush theory. The estimates of R_{12} obtained from the TD-DFT values of $\mu_\pm$ and from the experimental values of μ_{12} are given in Table 4. As expected, R_{12} approaches R when the electronic coupling decreases.

Recently, the ET distance in several organic MV systems has been investigated by means of AM1 calculations of the ground-state dipole moment.[19,20] In this approach, $\Delta\mu_{12}$ is obtained as twice the ground-state dipole moment, provided the coordinate system is correctly located on the molecular center of symmetry. The application of this approach in our case is complicated by the fact that the value of the dipole moment strongly depends on the method used for geometry optimization. For example, the DFT calculation results in a nearly symmetric configuration close to that obtained with symmetry constraints and thus yields a very small value of the dipole moment; for instance, $\Delta\mu_{12} =$ 0.5 D for system $\mathbf{3}^+$. This value is in contradiction with the above estimate based on TD-DFT and experimental results. At this stage, it is not clear whether this discrepancy is a consequence of the neglect of solvent effect in the DFT optimizations or is due to the nature of the DFT exchange-correlation functionals,[38] that sometimes lead to an overstabilization of delocalized states.

Table 5. Relaxation Energies L (cm^{-1}) of Systems $\mathbf{1}^+-\mathbf{4}^+$ Obtained from DFT and TD-DFT Calculations

	$\mathbf{1}^+$	$\mathbf{2}^+$	$\mathbf{3}^+$	$\mathbf{4}^+$
DFT(ES)[a]	2083	1383	873	931
DFT(GS)[b]	1978	1175	839	678
TD-DFT	1673	1206	738	627

[a] From the excited-state (ES) adiabatic potential surface. [b] From the ground-state (GS) adiabatic potential surface.

In contrast to DFT, the HF optimizations result in an asymmetric geometry with large dipole moments. For system $\mathbf{3}^+$, $\Delta\mu_{12}$ calculated at the ab initio UHF/6-31G** level is 50.6 D, in good agreement with the value of 48.8 D obtained previously by Lambert and Nöll[17] at the AM1-UHF level. The value of $\Delta\mu_{12} = 50.6$ D yields $R_{12} = 10.5$ Å; this is twice larger than our estimate $R_{12} = 4.92$ Å and even significantly larger than the TD-DFT diabatic ET distance $R = 6.89$ Å. In this context, it is worth noting that the conventional HF methods based on single-configuration wave functions fail for the radical-cation state of tryarilamine systems,[22] as was already noted for many other open-shell systems.[38] The ab initio UHF calculations as well as the AM1-UHF calculations suffer from a high amount of spin contamination (for instance, for system $\mathbf{3}^+$ at the UHF/6-31G** level $\langle S^2\rangle = 3.1$), which strongly questions their reliability. We also stress that, as in the case of eq 20, the relation given by eq 26 is only valid in the adiabatic limit.

5. Relaxation Energy. We have estimated the relaxation energy L and consequently the diagonal vibronic constant from geometry optimizations of the ground and excited states. To optimize the geometry of the excited state, we have used the same procedure as for the calculation of the electronic coupling parameter at the DFT level that exploits the symmetry properties of the electronic wave functions. L has been calculated from the adiabatic potential surface of the ground state (GS) and from that of the excited state (ES); if the force constants associated with these surfaces are equal, both calculations should yield the same result; see Figure 3. Additionally, we have estimated the relaxation energy as one-half the difference of the TD-DFT excitation energies obtained at the respective equilibrium geometries of the ground and first excited electronic states. The calculated values of L are collected in Table 5.

It is clear that the relaxation energy is significant for all systems. The DFT and TD-DFT estimates are in very good mutual agreement. Table 5 indicates that the relaxation energies obtained using the adiabatic surface of the excited state are always somewhat larger than those obtained from the adiabatic surface of the ground state; this implies a larger force constant for the excited state. This difference is larger for systems $\mathbf{2}^+$ and $\mathbf{4}^+$; this is apparently a symmetry effect, because the

(38) Bally, T.; Borden, W. T. *Rev. Comput. Chem.* **1999**, *13*, 1.

symmetry of the lowest states in compounds $\mathbf{2}^+$and $\mathbf{4}^+$ is reversed with respect to compounds $\mathbf{1}^+$ and $\mathbf{3}^+$.

IV. Discussion of the Application of Vibronic Theory

Systems $\mathbf{1}^+-\mathbf{4}^+$ exhibit a rather intense CT transition. Using the experimental values for the transition dipole moments,[17] we estimated the oscillator strengths of the CT transitions to be 0.38, 0.40, 0.39, and 0.15, respectively. For comparison, the oscillator strength of the Creutz−Taube ion,[9] that is considered as a class III system, is about 0.03. Thus, these intensities are an experimental indication that the electronic coupling in these systems is strong. In addition, the bands in the triarylamine systems are significantly broader than those in the ruthenium compound; the implication is that the vibronic interactions are also very strong in our systems.

Our electronic-structure calculations provide results in good agreement with the experimental data. To allow a quantitative comparison, the electronic parameters have been evaluated from the spectroscopic data. For this purpose, we have first solved the dynamic vibronic problem. The resulting eigenfunctions and eigenvalues have been then used to simulate the CT band. The numerical calculations have been performed using the TD-DFT values of the transition dipole moment $\mu_{\pm}$ and of the relaxation energy L. The energy $\hbar\omega_+$ of the symmetric vibrational mode was set to 1050 cm^{-1}, a value that is in the region of the C−N stretching in triarylamine molecules.[39] Note that as mentioned in section III.2, this bond is the one that undergoes the largest relaxation upon excitation of the cation. The energy $\hbar\omega_-$ of the antisymmetric vibrational mode has been taken as 500 cm^{-1} for $\mathbf{1}^+$, 300 for $\mathbf{2}^+$ and $\mathbf{3}^+$, and 200 cm^{-1} for $\mathbf{4}^+$. This choice for the $\hbar\omega_-$ energies is justified by the fact that ω_- is an effective mode that accounts for the overall effect of the low energy solvent modes and of all the intramolecular modes coupled to the ET process. The decrease of ω_- for the systems with larger bridge accounts for the experimental evidence[17] of an increasing role of solvent interactions in the total reorganization process. The reorganization energy parameters and the electronic coupling constants have been obtained by fitting the position, intensity, and shape of the theoretical CT band to the experimental spectra.

The calculated spectra are given in Figures 7−10. The CT bands have been simulated assuming Gaussian line shapes $\delta_i(E) = (1/\Gamma_i\pi^{1/2}) \exp[-(E - E_i)^2/\Gamma_i^2]$ for each vibronic peak. Γ_i is taken to be the same for all vibronic contributions and is chosen large enough to produce smooth bands. In Figures 7−10, the experimental bands[17] are compared to the fits obtained when considering (i) only the nondiagonal, vibronic interactions; (ii) only the diagonal vibronic interactions; or (iii) both interactions. Note that case (i) corresponds to the PKS approach, the dynamic equivalent of the Hush model. A nice fit is observed for all of the molecules when considering both diagonal and nondiagonal vibronic couplings. We now turn to a discussion of the relative importance of these two couplings.

We recently showed for $\mathbf{1}^+$ that the PKS model (interaction with an antisymmetric mode) is able to reproduce the major features of the CT band, that is, the position, intensity, bandwidth, and band asymmetry. However, some disagreements subsist when using this model. For instance, the smooth decrease on the high-energy side of the CT band is not well reproduced.

(39) Pacansky, J.; Waltman, R. J.; Seki, H. *Bull. Chem. Soc. Jpn.* **1997**, *70*, 55.

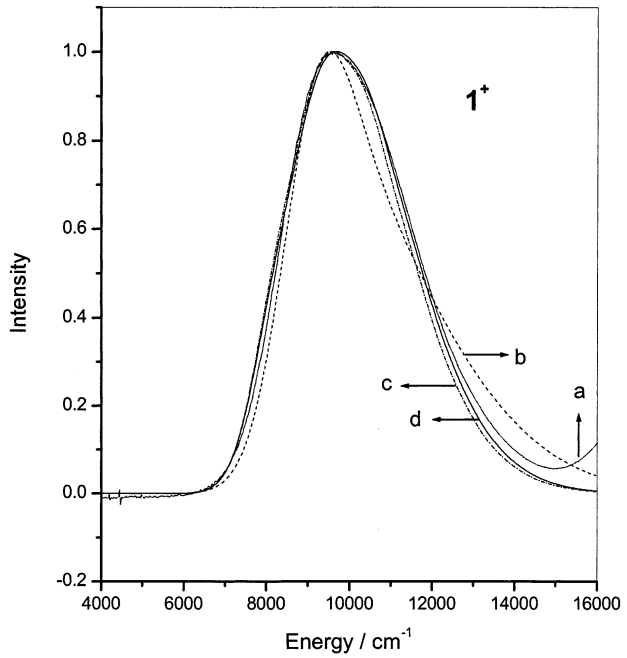

Figure 7. Calculated absorption profiles of $\mathbf{1}^+$ for the following sets of parameters: (a) experimental absorption spectrum taken from ref 17; (b) $\Delta = 8800$ cm^{-1}, $\lambda = 10\,950$ cm^{-1} with nondiagonal vibronic interactions; (c) $\Delta = 9950$ cm^{-1}, $\lambda = 0$ with diagonal vibronic interactions; (d) $\Delta = 9680$ cm^{-1}, $\lambda = 6500$ cm^{-1} with both diagonal and nondiagonal vibronic interactions.

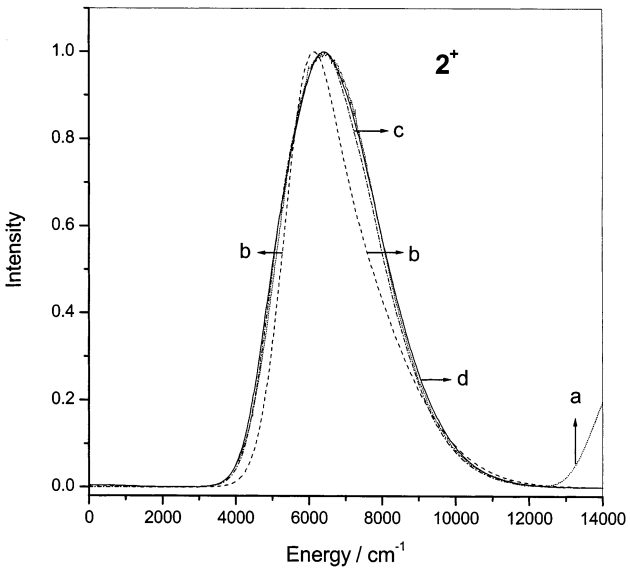

Figure 8. Calculated absorption profiles of $\mathbf{2}^+$ for the following sets of parameters: (a) experimental absorption spectrum taken from ref 17; (b) $\Delta = 5600$ cm^{-1}, $\lambda = 7000$ cm^{-1} with nondiagonal vibronic interactions; (c) $\Delta = 6600$ cm^{-1}, $\lambda = 0$ with diagonal vibronic interactions; (d) $\Delta = 6200$ cm^{-1}, $\lambda = 5000$ cm^{-1} with both diagonal and nondiagonal vibronic interactions.

We suggested[22] that a better description could be obtained by including symmetric vibrations. Indeed, our present electronic-structure calculations indicate a significant diagonal vibronic interaction in $\mathbf{1}^+$. As seen from Figure 7c, the model that includes only the diagonal vibronic contribution reproduces remarkably well the shape of CT band, in contrast to the PKS model. In fact, the inclusion of the contribution of the antisymmetric mode has little effect on the band shape as long as $\Delta > \lambda$ (see Figure 7d). However, the increase of this interaction yields

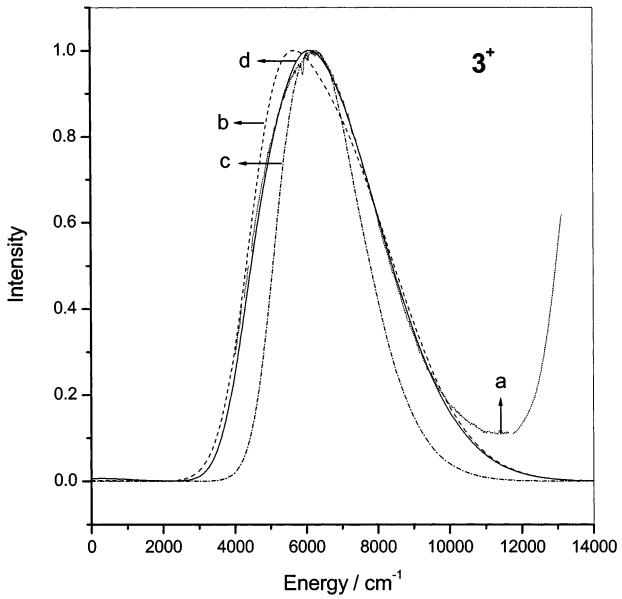

Figure 9. Calculated absorption profiles of $\mathbf{3}^+$ for the following sets of parameters: (a) experimental absorption spectrum taken from ref 17; (b) $\Delta = 4600\ cm^{-1}$, $\lambda = 7200\ cm^{-1}$ with nondiagonal vibronic interactions; (c) $\Delta = 6500\ cm^{-1}$, $\lambda = 0\ cm^{-1}$ with diagonal vibronic interactions; (d) $\Delta = 5100\ cm^{-1}$, $\lambda = 5900\ cm^{-1}$ with both diagonal and nondiagonal vibronic interactions.

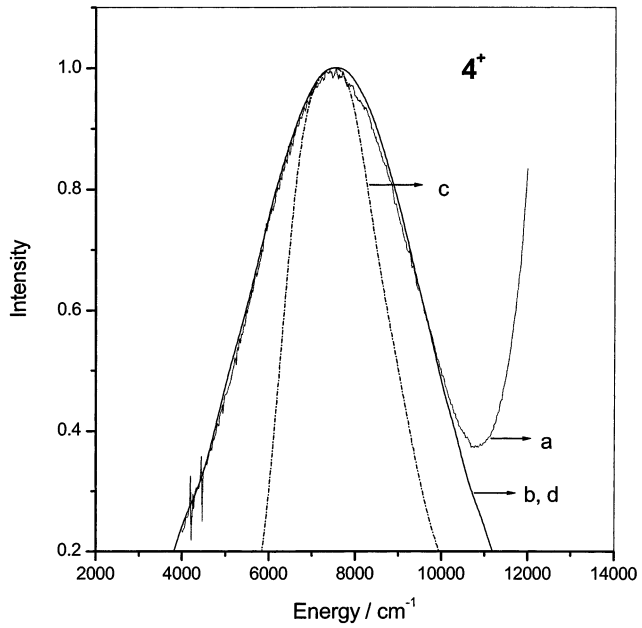

Figure 10. Calculated absorption profiles of $\mathbf{4}^+$ for the following sets of parameters: (a) experimental absorption spectrum taken from ref 17; (b) $\Delta = 3000\ cm^{-1}$, $\lambda = 8150\ cm^{-1}$ with nondiagonal vibronic interactions; (c) $\Delta = 7700\ cm^{-1}$, $\lambda = 0$ with diagonal vibronic interactions; (d) $\Delta = 3300\ cm^{-1}$, $\lambda = 8000 cm^{-1}$ with both diagonal and nondiagonal vibronic interactions.

a lower value for the electronic coupling; for instance, $\Delta = 9950\ cm^{-1}$ if $\lambda = 0$, and $\Delta = 9530\ cm^{-1}$ if $\lambda = 6500\ cm^{-1}$. Thus, our simulations of the CT spectra show that the electronic coupling in $\mathbf{1}^+$ is in the range $9500 \pm 500\ cm^{-1}$, which is in good agreement with the electronic-structure estimates. Because when $\Delta > \lambda$ the theoretical CT band is not very sensitive to the reorganization energy, we are not able to draw a definite conclusion about the λ value, but we are confident that λ/Δ is smaller or very close to 1; if $\lambda/\Delta \gg 1$, the theoretical band would no longer match the experimental one.

The same trends are observed for system $\mathbf{2}^+$. Interestingly, the experimental bandwidth, $\nu_{1/2} = 3170\ cm^{-1}$, is smaller in this case than the one observed in $\mathbf{1}^+$, $\nu_{1/2} = 4640\ cm^{-1}$. Our TD-DFT estimates indicate that in going from $\mathbf{1}^+$ to $\mathbf{2}^+$ the relaxation energy drops from $L = 1673\ cm^{-1}$ to $L = 1206\ cm^{-1}$; taking this latter value provides a good simulation of the CT band (see Figure 8c). As for $\mathbf{1}^+$, the simulations based on the two-mode model with a fixed TD-DFT relaxation energy reveal that the reorganization energy is smaller or at least does not significantly exceed the electronic coupling parameter. A good fit is obtained with the parameters $\Delta = 6200\ cm^{-1}$ and $\lambda = 5000\ cm^{-1}$. The theoretical estimate of the oscillator strength ($f = 0.56$) is larger than the experimental one ($f = 0.4$). This might indicate either an underestimation of the ratio λ/Δ or an overestimation of the transition dipole moments $\mu_{\pm}$. Therefore, further calculations of the $\mu_{\pm}$ term that account for solvent interactions are still needed to distinguish between these two cases.

In systems $\mathbf{3}^+$ and $\mathbf{4}^+$, the role of the diagonal and nondiagonal couplings is reversed with respect to $\mathbf{1}^+$ and $\mathbf{2}^+$. The shape (see curves c in Figures 9 and 10) and intensity of the CT bands are not reproduced by considering only the diagonal coupling. For instance, the oscillator strength for system $\mathbf{4}^+$ considering only the diagonal coupling is calculated as $f = 1.29$, one order of magnitude larger than the experimental value (0.15). In contrast, the PKS model reproduces satisfactorily the experimental shape in $\mathbf{3}^+$ and performs remarkably well in $\mathbf{4}^+$. In $\mathbf{3}^+$, a good fit is achieved in the two-mode model by using $\Delta = 5100\ cm^{-1}$ when $\lambda = 5900\ cm^{-1}$. This set of parameters yields $f = 0.48$ to be compared with an experimental value $f = 0.39$. The electronic coupling parameter is in the range of the electronic-structure estimates, though smaller than the TD-DFT prediction. An interesting feature of $\mathbf{3}^+$ is that the reorganization energy is now found to be definitely larger than the electronic coupling. This means that, according to our model, systems $\mathbf{2}^+$ and $\mathbf{3}^+$ should be located on opposite sides of the borderline between class III and class II. We note, however, that further experimental and theoretical studies of the solvent and intramolecular multimode effects are still needed to draw more definite conclusions on the electron delocalization pattern in these systems.

In $\mathbf{4}^+$, the shape of the CT band is completely dominated by the nondiagonal vibronic coupling. This model reproduces very well the shape of the CT band for $\Delta = 3000\ cm^{-1}$ when $\lambda = 8150\ cm^{-1}$. The fitting within a two-mode model changes these parameters only slightly ($\Delta = 3300\ cm^{-1}$ when $\lambda = 8000\ cm^{-1}$). In contrast to the previous systems, the dynamic vibronic model yields a significantly smaller value for the electronic coupling than the one evaluated from the electronic-structure calculations. At this stage, the origin of this discrepancy is not clear. The calculated oscillator strength of 0.19 slightly overestimates the experimental value, 0.15.

Conclusions

We have performed electronic-structure calculations on MV triarylamine compounds in an attempt to clarify the nature of the lowest optical transitions. Our study supports the assignment of the lowest optical band in these systems as the CT transition.

This band, however, presents a more complex nature than in traditional inorganic MV systems. In fact, in the triarylamines, the CT transition cannot be associated simply with an electron-transfer process because it also contains a contribution that corresponds to a charge density shift from the terminal phenylene rings to the central part of the molecule. We expect that this feature can contribute to the solvent dependence of CT transitions.

The shape of the CT bands has been simulated using a two-mode dynamic vibronic model. The numerical simulation reveals that the band shape results from a subtle balance between the diagonal and nondiagonal vibronic interactions. The role of diagonal vibronic coupling is dominant in $\mathbf{1}^+$ and decreases from $\mathbf{1}^+$ to $\mathbf{4}^+$, that is, as the length of the central bridge increases. The nondiagonal vibronic coupling exhibits an opposite trend. To the best of our knowledge, the present work constitutes the first study where the interplay of diagonal and nondiagonal vibronic interactions has been considered for an MV organic system. Our results fully support Hush's prediction on the dominant role of symmetric vibrations in determining the band shape in delocalized MV systems.

Our simulations of the shape of the CT band indicate a broken-symmetry effect for $\mathbf{3}^+$ to $\mathbf{4}^+$; thus, these systems can be classified as class II systems. Although it is not possible to draw a definite conclusion about the ratio λ/Δ for $\mathbf{1}^+$ and $\mathbf{2}^+$, the simulations based on the two-mode model reveal that the reorganization energy is smaller or at least does not significantly exceed the electronic coupling parameter; thus, $\mathbf{1}^+$ and $\mathbf{2}^+$ can be classified as class II−class III borderline systems.

The electronic coupling parameters estimated from the electronic-structure calculations and the vibronic coupling simulations of the CT bands for $\mathbf{1}^+$, $\mathbf{2}^+$, and $\mathbf{3}^+$ are in a good agreement. In the case of $\mathbf{4}^+$, which has the longest central bridge, the TD-DFT estimate is about twice as large as that obtained from the dynamic vibronic simulations. Investigations to understand the origin of this discrepancy are currently in progress.

Acknowledgment. This work is supported by the National Science Foundation (CHE-0078819), the Office of Naval Research, and the IBM Shared University Research Program. J.M.A. is also indebted to the Belgian National Fund for Scientific Research (FNRS) for partial support of his stay at the University of Arizona. The authors thank Professor C. Lambert for stimulating discussions.

JA026437J